High-precision half-life determination for ^{21}Na using a 4π gas-proportional counter

P. Finlay,[1,*] A. T. Laffoley,[2,†] G. C. Ball,[3] P. C. Bender,[3,‡] M. R. Dunlop,[2] R. Dunlop,[2] G. Hackman,[3] J. R. Leslie,[4] A. D. MacLean,[2] D. Miller,[3,§] M. Moukaddam,[3,‖] B. Olaizola,[2] N. Severijns,[1] J. K. Smith,[3,¶] D. Southall,[3] and C. E. Svensson[2]

[1]*K.U. Leuven, Instituut voor Kern- en Stralingsfysica, Celestijnenlaan 200D, 3001 Leuven, Belgium*

[2]*Department of Physics, University of Guelph, Guelph, Ontario N1G 2W1, Canada*

[3]*TRIUMF, 4004 Wesbrook Mall, Vancouver, British Columbia V6T 2A3, Canada*

[4]*Department of Physics, Queen's University, Kingston, Ontario K7L 3N6, Canada*

(Received 13 January 2017; published 9 August 2017)

A high-precision half-life measurement for the superallowed β^+ transition between the isospin $T = 1/2$ mirror nuclei ^{21}Na and ^{21}Ne has been performed at the TRIUMF-ISAC radioactive ion beam facility yielding $T_{1/2} = 22.4506(33)$ s, a result that is a factor of 4 more precise than the previous world-average half-life for ^{21}Na and represents the single most precisely determined half-life for a transition between mirror nuclei to date. The contribution to the uncertainty in the ^{21}Na $\mathcal{F}t^{\text{mirror}}$ value due to the half-life is now reduced to the level of the nuclear-structure-dependent theoretical corrections, leaving the branching ratio as the dominant experimental uncertainty.

DOI: 10.1103/PhysRevC.96.025501

I. INTRODUCTION

Measurements of superallowed β-decay transitions between isospin $T = 1$ multiplets have proven to be an invaluable probe of the standard electroweak model. These transitions currently provide the most precise limits on weak scalar currents coupling to left-handed neutrinos [1], have verified the conservation of the vector weak current (CVC) to better than 12 parts in 10^5, and collectively provide the most precise determination of V_{ud}, the up-down element of the Cabibbo-Kobayashi-Maskawa (CKM) quark-mixing matrix and the leading term in the top-row unitary sum [2]. Over 200 individual measurements currently contribute to the most precise superallowed Fermi $\mathcal{F}t$ values from which V_{ud} is derived, making this a very robust data set whose precision is currently limited by small theoretical corrections rather than experimental uncertainties. Efforts to improve the precision in V_{ud} have thus expanded recently to include the set of superallowed transitions within isospin $T = 1/2$ multiplets know as mirror nuclei [3], which currently provide the second most precise value for V_{ud} and whose uncertainty is dominated by the experimental, rather than theoretical, contributions. For isospin $T = 1/2$ mirror decays, V_{ud} is related to the $\mathcal{F}t^{\text{mirror}}$ value via [4]:

$$\mathcal{F}t^{\text{mirror}} = \frac{K}{G_F^2 V_{ud}^2} \frac{1}{\left(1 + \Delta_R^V\right)\left(1 + \frac{f_A}{f_V}\rho^2\right)}, \tag{1}$$

where $K/(\hbar c)^6 = 2\pi^3 \hbar \ln 2/(m_e c^2)^5 = 8120.2776(9) \times 10^{-10}\,\text{GeV}^{-4}\,\text{s}$, $G_F/(\hbar c)^3 = 1.1663787(6) \times 10^{-5}\,\text{GeV}^{-2}$ [5] is the Fermi constant, f_A and f_V are statistical rate functions for the axial-vector and vector currents, respectively, ρ is the Gamow-Teller to Fermi mixing ratio, and Δ_R^V is a nucleus-independent radiative correction. Since the axial-vector current is not conserved in β decay the mixing ratio ρ must be determined experimentally on a case-by-case basis.

In order to relate $\mathcal{F}t^{\text{mirror}}$ to the experimental mirror $f_V t$ value further corrections for radiative and nuclear-structure effects must be considered:

$$\mathcal{F}t^{\text{mirror}} \equiv f_V t(1 + \delta_R')\left(1 + \delta_{NS}^V - \delta_C^V\right). \tag{2}$$

The terms δ_R' and δ_{NS}^V are the transition-dependent components of the radiative correction, and δ_C^V is the isospin-symmetry-breaking correction [4], where the superscript V indicates these corrections are for the vector part of the transition. Calculations for the nuclear-structure-dependent corrections δ_{NS}^V and δ_C^V are also required to extract V_{ud} from the $T = 1$ superallowed Fermi ft values, and these calculations currently contribute the largest uncertainty in the $T = 1$ world-average superallowed Fermi $\mathcal{F}t$-value error budget. The $\mathcal{F}t^{\text{mirror}}$ values, on the other hand, are dominated by the uncertainties in the experimental quantities, and there is thus a strong motivation to pursue a reduction in the uncertainties in the mirror $f_V t$ values. Ultimately, a precise test of CVC in the superallowed mirror decays, where the nuclear structure differs from the pure Fermi emitters, would provide a demanding test of the consistency of the nuclear-structure-dependent corrections δ_{NS}^V and δ_C^V, and would thus contribute to an improved determination of V_{ud} from the superallowed Fermi emitters as well.

In this paper, we present a half-life measurement for the $T = 1/2$ mirror nucleus ^{21}Na, which, with an uncertainty of 0.015%, represents the most precisely measured half-life for a mirror transition to date. This high-precision result calls into question a recent precision measurement [6] that is at odds with both the result presented here and earlier less precise measurements [7,8]. This emphasizes the need for a large and

*pfinlay314@gmail.com

†Present address: GANIL, CEA/DSM-CNRS/IN2P3, Bvd Henri Becquerel, 14076 Caen, France.

‡Present address: NSCL, 640 S. Shaw Ln, East Lansing, Michigan 48824, USA.

§Present address: Idaho National Laboratory, Idaho Falls, Idaho 83415, USA.

‖Present address: University of Surrey, Guildford GU2 5XH, United Kingdom.

¶Present address: Reed College, 3203 SE Woodstock Blvd, Portland, Oregon 97202, USA.

robust set of mirror $f_V t$ values before a precise, and accurate, value for V_{ud} can be determined from these transitions.

II. EXPERIMENT

The experiment was performed at TRIUMF's Isotope Separator and Accelerator (ISAC) facility [9] where the ^{21}Na was produced by bombarding a high-powered tantalum target with 70 μA of 480 MeV protons from the main cyclotron. The spallation products diffused from the target and were surface ionized, mass separated to isolate the singly ionized $A = 21$ products, and then delivered as a 30 keV beam at a rate of up to 9×10^4 ^{21}Na/s to the experimental station.

The beam was implanted under vacuum into a Mylar tape with a 17.2 μm thick aluminum layer for 4–10 s, after which the beam was deflected at the mass separator and the portion of tape containing the ^{21}Na activity was moved for ~2 s to bring the sample to the center of a 4π continuous-flow gas proportional counter [10]. The activity was measured with the counter for up to 550 s (~24 ^{21}Na half-lives) before a new sample was implanted and the cycle repeated. The amplified pulses from the counter were discriminated and then fanned into two LeCroy 222N nonretriggerable gate-and-delay generators providing independent fixed, nonextendable dead times of approximately 3 μs and 4 μs for each data stream. These fixed dead times were measured via the source-plus-pulser technique [11] both immediately before and after the experiment, resulting in $\tau_1 = 4.009 \pm 0.018\,\mu$s and $\tau_2 = 2.997 \pm 0.018\ \mu$s, respectively. The dead-time-affected data were registered by two independent multichannel scaler (MCS) modules into 500 channels with dwell times between 0.9 and 1.1 s, with a Stanford Research Systems model DS335 1 MHz ± 2 Hz temperature-stabilized clock providing the time standard. The detector high voltage, discriminator level, and dwell time were varied run-by-run and the outputs of the gate-and-delay generators were periodically swapped between the two MCS units to investigate potential systematic effects.

The gas counter was operated within its plateau region between 2340 V and 2500 V, previously determined via off-line measurements with ^{90}Sr β sources [10]. Following the ^{21}Na half-life measurements a beam of ^{66}Ga ($T_{1/2} = 9.49(3)$ h [12], $Q_{EC} = 5175.0(32)$ keV [13]) was used to characterize the gas counter, as this source more closely resembles the decays of typical nuclei being measured with this facility (i.e., a β^+ emitter having a several MeV Q_{EC} value). A beam of 2×10^4 ^{66}Ga/s was implanted into the aluminized Mylar tape for ~2 hours in order to build up a suitably intense source, which was then allowed to cool for approximately one hour in order to remove the isobaric contaminant ^{66}Cu ($T_{1/2} = 5$ min) before the pure source of ^{66}Ga was moved to the center of the gas counter.

The measured activity, corrected for the decay of ^{66}Ga, is shown in Fig. 1 as a function of detector bias voltage. A linear regression on the plateau region between 2300 V and 2500 V yields slopes of 0.100(21) cps/V and 0.065(25) cps/V for the 115 mV and 70 mV discriminator data, respectively. The gas counter high-voltage unit is a Power Designs Model 1570 with a quoted voltage stability of 0.001% over a one hour period. At the highest voltage setting of 2500 V this implies

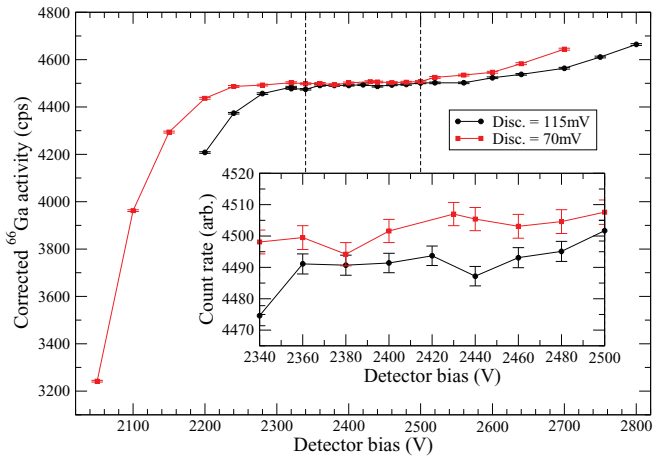

FIG. 1. Voltage plateau measurements for the 4π gas counter at the highest (black circles) and lowest (red squares) discriminator settings used in this experiment, with lines connecting the data points drawn to aid the eye. The voltage range over which the detector was operated for the ^{21}Na half-life measurements is bracketed by vertical dashed lines and shown in the inset.

a potential fluctuation in the counting rate of ±0.0025 cps and ±0.0016 cps for the 115 mV and 70 mV discriminator settings, respectively. As our maximum cycle length for the ^{21}Na half-life measurement is only 550 s these already small fluctuations would be further reduced, and it is thus reasonable to treat the counting rate as voltage independent over this region of operation of the gas counter.

Potential contaminants in the ^{21}Na beam were investigated by placing an 80% relative efficiency HPGe detector next to the counter and recording γ-ray events in coincidence with βs registered in the gas detector over the course of the experiment. The resulting $\beta\gamma$-coincident spectrum, summed for all ^{21}Na half-life runs, is displayed in Fig. 2 and shows no evidence for any in-beam contamination.

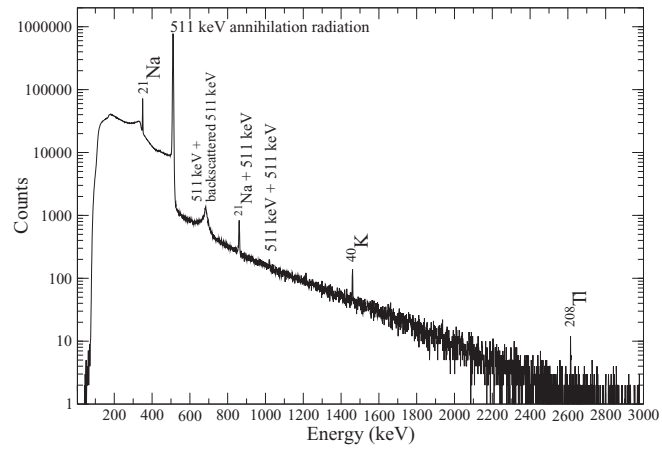

FIG. 2. β-coincident γ-ray spectrum summed for all ^{21}Na half-life runs, with the origin of the γ-ray peaks labeled. No transitions from nuclei other than ^{21}Na and room background are identifiable.

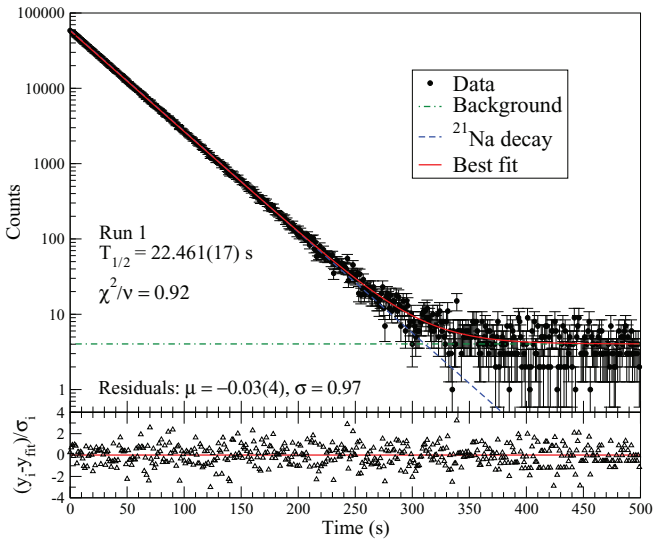

FIG. 3. Decay data from a typical run composed of five cycles, with fit overlaid and residuals (bottom). The mean and sigma of the residuals, and the χ^2/ν for the fit, are consistent with normally distributed data.

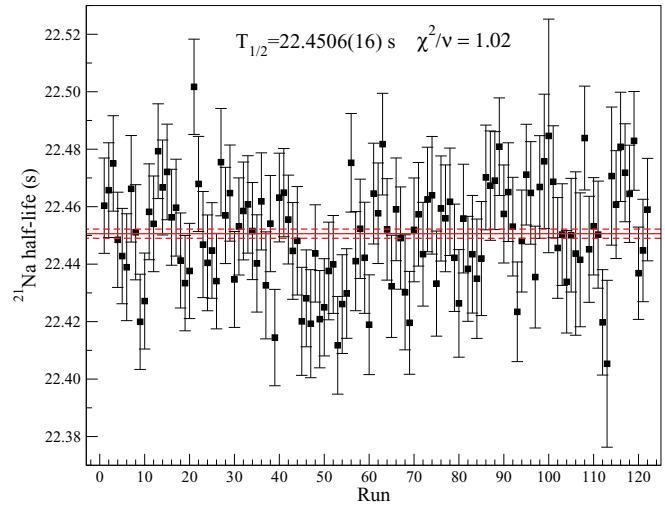

FIG. 4. Deduced ^{21}Na half-lives for each experimental run, with the weighted average and $\pm 1\sigma_{\text{stat}}$ limits indicated by the solid and dashed red lines, respectively. The χ^2/ν of 1.02 indicates excellent statistical consistency amongst the resulting half-lives.

III. ANALYSIS

A total of 620 ^{21}Na half-life measurement cycles spread over 122 runs with different experimental conditions were recorded. Of these, 28 cycles were rejected due to a proton trip during implantation resulting in insufficient statistics for that cycle, or due to a burst of electronic noise, typically associated with the LN2 filling system of a neighboring spectrometer. These rejected cycles made up less than 3% of the total number of counts recorded during the experiment. The surviving cycles were dead-time corrected, then summed and fit run-by-run using a maximum-likelihood routine described in Refs. [14–16]. The fit function included an exponentially decaying ^{21}Na activity and a constant background with both activity parameters, as well as the ^{21}Na half-life, left as free parameters in the fit.

The decay data for a typical run, with fit overlayed and residuals, are displayed in Fig. 3. The statistical precision of 0.08% obtained in this single five-cycle run is comparable to the precision of the previous world-average ^{21}Na half-life [6]. The weighted average of the fit results for all 122 runs, displayed in Fig. 4, yields a value for the ^{21}Na half-life of $22.4506 \pm 0.0016_{\text{stat}}$ s and a χ^2/ν of 1.02, indicating a statistically consistent data set.

A. Systematics

The accuracy of the frequency generator providing the time standard was verified by the RF group at TRIUMF one year prior to the experiment, and was also remeasured recently to explore long-term stability. The frequency generator was found to be approximately 2 ppm slower than quoted by the manufacturer. The impact of this on the deduced ^{21}Na half-life was assessed by increasing the nominal bin times by 2 ppm and refitting the half-life runs. The increased bin times were found to have no impact on the deduced ^{21}Na half-life, and the nominal bin times were thus used in the final analysis.

An $A = 21$ contaminant potentially overlooked in the γ-ray analysis is ^{21}F ($T_{1/2} = 4.158$ s), as it also feeds the 350 keV level in ^{21}Ne, which is fed in the ^{21}Na decay, producing a 350 keV γ ray. To check for potential contamination from ^{21}F the expected location of the 1395 keV γ ray (produced in 15.3% of ^{21}F decays) was fit with a fixed centroid and a width fixed from the fit to the neighboring 1460 keV γ ray from ^{40}K. The resulting peak area of -14 ± 16 counts for the 1395 keV γ ray is fully consistent with no ^{21}F present in the beam, as expected for the surface ion source used in this experiment. Nonetheless, as a negative intensity for this transition is clearly unphysical, to be conservative we integrate a Gaussian probability distribution with $\mu = -14$ and $\sigma = 16$ over positive counts from zero to infinity and define an upper limit on the potential ^{21}F contamination that includes 68% of this area. This yields a one-sigma upper limit of ten counts over the entire experiment, and a ^{21}F intensity relative to ^{21}Na of 5.6×10^{-5}. Including a ^{21}F component in the fitting routing with an intensity fixed at this value changes the deduced half-life for ^{21}Na by 3×10^{-4} s, and is thus negligible compared to the statistical uncertainty of 0.0016 s. The only other $A = 21$ isotope expected to be ionized by the surface ion source used in this experiment is ^{21}Mg, with an intensity orders of magnitude below the readily surface ionized, and longer lived, ^{21}Na beam of interest. ^{21}Mg differs in mass from ^{21}Na by approximately one part in 1500 and would thus also be suppressed by the mass separator. Furthermore, with a half-life of only 122 ms, any remaining ^{21}Mg contaminant in the beam would be suppressed by an additional factor of $\sim 10^5$ during the ~ 2 s tape move to the gas counter, consistent with the absence of any evidence for the 332 keV and 1384 keV γ rays following ^{21}Mg decay in the spectrum of Fig. 2.

In order to investigate any dependence of the deduced ^{21}Na half-life on the initial rate in the gas counter, the individual

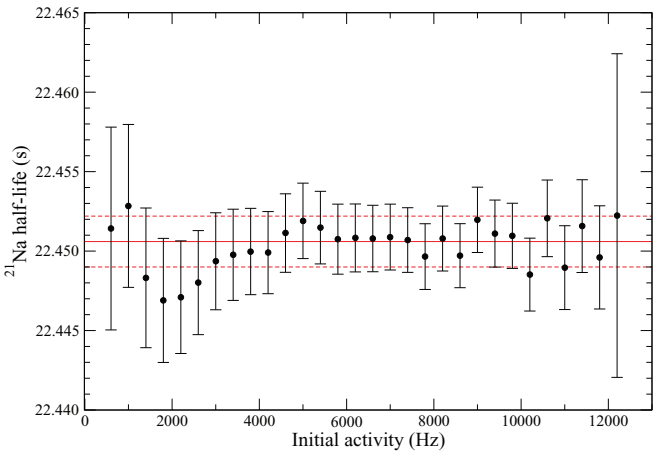

FIG. 5. Weighted averages of the ^{21}Na half-life values obtained from fits to the cycles with leading channels removed. Resulting half-lives were averaged when the ^{21}Na activity at the beginning of the fit was equal to within ± 200 Hz of the value indicated on the x axis. The data points are strongly correlated since individual cycles contribute to multiple data points, however, no cycle contributes more than once to any individual data point.

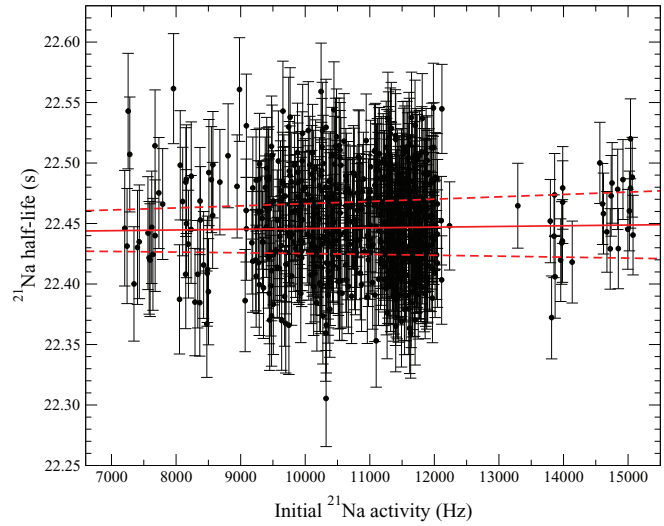

FIG. 6. The deduced cycle-by-cycle ^{21}Na half-lives plotted as a function of the measured initial ^{21}Na activity. The slope obtained from a linear regression yields $5.8 \pm 11.6 \times 10^{-7}$ s/Hz, a value consistent with zero indicating no systematic associated with the initial rate in the gas counter.

cycles were fit repeatedly with an additional leading channel removed upon each iteration. The resulting half-life values for which the initial ^{21}Na activities were equal to within ± 200 Hz were then combined in a weighted average. If, upon chopping a subsequent leading channel, the activity was not reduced by more than 200 Hz, then the half-life obtained from that particular chop was not included. In this way, an individual cycle contributes no more than once to each data point in Fig. 5. For example, if the ^{21}Na activity at the beginning (zero channels removed) of a particular cycle was 10 kHz, then this particular cycle would contribute to every data point in Fig. 5 whose corresponding x value is less than or equal to 10 kHz once leading channels are removed from this cycle. It should be noted that a weighted average of half-lives obtained from low-statistics measurements can bias the average towards lower half-life values [17]. This analysis was thus repeated on the run-by-run data and produced similar results, validating the procedure used to generate Fig. 5. The consistency in this plot indicates that there is no systematic bias in the resulting ^{21}Na half-life deduced at either high or low initial activities in the gas counter. Rate dependence was further explored by fitting the deduced cycle-by-cycle ^{21}Na half-life as a function of the initial ^{21}Na activity. The fit result, shown in Fig. 6, is consistent with no systematic trend (zero slope) in the ^{21}Na half-life with initial rate in the gas counter. Although the cycle-by-cycle data was used for these particular rate-dependence tests, we reiterate that the cycles from each run were dead-time corrected and then summed and fit in order to produce the final result for the ^{21}Na half-life reported in this paper.

To further explore potential systematic effects, the run-by-run half-lives were grouped according to experimental conditions as shown in Fig. 7. During the experiment the detector voltage was varied between 2340 V and 2500 V, within its plateau region (see Fig. 1), the threshold for the discriminator was adjusted between 70 mV and 115 mV in 15-mV steps, while the dwell time for the MCS bins, and hence the total length of the counting period of the cycle, was varied between 0.9 s/bin, 1.0 s/bin, and 1.1 s/bin, or 450 s, 500 s, and 550 s of counting, respectively. The resulting half-lives from the two independent MCS units, and measured for each of the two fixed dead times, are consistent with one another, as are the results when grouped according to the discriminator settings. The half-life groupings according to detector voltage and dwell time, however, yield χ^2/ν of 2.5 and 3.6, respectively. For $\nu = 4$ and $\nu = 3$ degrees of freedom, the statistical probability of obtaining χ^2/ν values this large or larger are 4% and 1%, respectively.

While no systematic trend to the deduced half-lives is discernible in the bias-voltage grouping, an argument could be made that the first three points in the dwell-time grouping indicate a dwell-time-dependent systematic effect, i.e., the

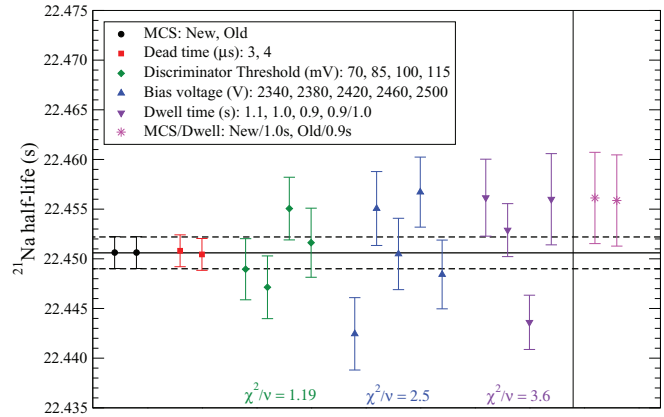

FIG. 7. Half-life measurements grouped according to experimental parameters. See text for details.

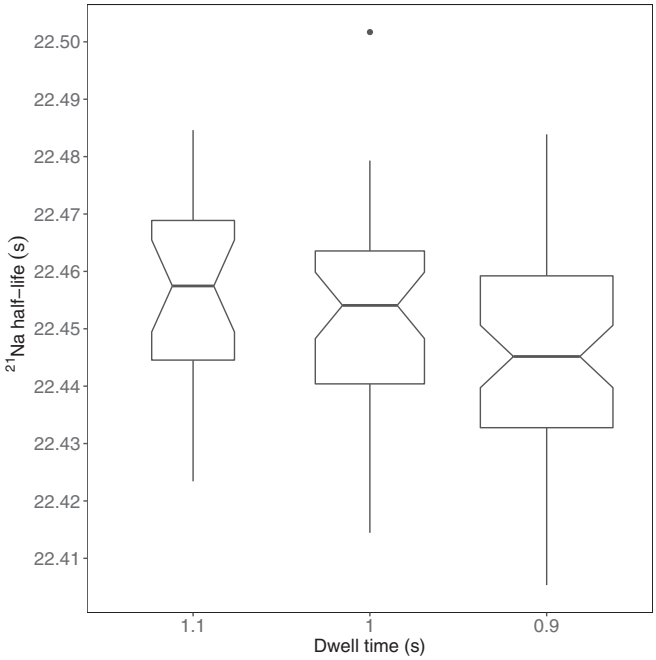

FIG. 8. Box plots for the run-by-run half-lives measured with the new MCS grouped according to the dwell-time parameter. The horizontal line through each box is the median of the distribution, while the vertical extent of the box encompasses the interquartile range (25% to 75% of the distribution). The error bars extend to 1.5 times the interquartile range, after which data is rendered as discreet points. The width of each box is proportional to the square root of the number of runs measured at that dwell setting, while the notches represent the 95% confidence interval of the median.

deduced half-life could depend on how much background is included in the fit. This possibility was explored during the analysis by removing bins from the end of the activity curves for the 1.0 s and 1.1 s dwell-time data, with no significant change in the deduced ^{21}Na half-life observed. This potential systematic was explored further online by performing a set of ^{21}Na half-life measurements where one of the independent MCS units was operated with a dwell time of 0.9 s/bin, while the other was simultaneously operated with a dwell time of 1.0 s/bin. Since the half-lives from the two MCS units are found to be perfectly consistent with one another for the whole data set (see first grouping in Fig. 7), a discrepancy in the half-lives measured by the two MCS units being operated with different dwell times would confirm the presence of a dwell-time-dependent systematic effect. These data, labeled as "New/1.0 s" and "Old/0.9 s," are displayed at the end of Fig. 7. The half-lives measured simultaneously with different dwell-time settings, averaged to create the fourth point labeled "0.9/1.0" in the dwell-time grouping in Fig. 7, are perfectly consistent with one another, indicating that there is no systematic effect associated with the dwell-time settings.

The half-life distributions for the three dwell times are summarized in Fig. 8 as notched box plots, where the notches represent the 95% confidence interval of the median. A lack of overlap between notches for the distributions would be strong evidence that these distributions do not agree at the 95% confidence limit [18]. This is not observed for the dwell-time groupings of the half-lives and thus, while the χ^2/ν for these groupings indicates disagreement at the 1σ level, the distributions of half-lives across the different dwell times appear to be consistent with one another and lend further support to the hypothesis of a lack of systematic associated with this parameter.

While the analysis described above lends strong support to the hypothesis that there is no systematic associated with the dwell-time parameter, the large χ^2/ν for this grouping remains. In a conservative effort to avoid underestimating the uncertainty in the deduced ^{21}Na half-life we therefore adopt the Particle Data Group (PDG) convention [5] and inflate our statistical uncertainty by $\sqrt{\chi^2/\nu} = \sqrt{3.6} = 1.90$, resulting in a systematic uncertainty of ± 0.0026 s, which is added in quadrature with our statistical uncertainty of ± 0.0016 s.

A final systematic to account for the uncertainty in the measured dead times was determined by refitting the half-life data with the dead times fixed at their $\pm 1\sigma$ limits. Taking half the difference in the half-lives determined in this manner yields a systematic uncertainty associated with the measured dead times of ± 0.0012 s, and a final result for the half-life of ^{21}Na from this paper of:

$$\begin{aligned} T_{1/2} &= 22.4506 \pm 0.0016_{\text{stat}} \pm 0.0029_{\text{syst}}\text{s} \\ &= 22.4506(33)\text{s}. \end{aligned} \tag{3}$$

This result is a factor of 4 more precise than the current world-average half-life for ^{21}Na, and at $\pm 0.015\%$ is the most precise measurement for a mirror half-life yet reported.

IV. RESULTS AND DISCUSSION

The result reported here is in excellent agreement with, but 16 times more precise than, the world-average ^{21}Na half-life of $T_{1/2} = 22.487(54)$ s reported in the most recent review of $\mathcal{F}t^{\text{mirror}}$ values [4]. That average has since been updated with the addition of a high-precision measurement (Gr15) [6] in agreement with the aforementioned average at only the 2σ level. With the addition of the result reported here, the weighted average of the four most precise ^{21}Na half-life values is $T_{1/2} = 22.448(5)$ s, where the uncertainty has been inflated by a factor of 1.73 as per the PDG prescription due to the large $\chi^2/\nu = 3.0$ for this set of half-lives (see Fig. 9).

The standard adopted when evaluating the world-averaged $T = 1$ and $T = 1/2$ superallowed data is to include a measurement only if the uncertainty in that value is less than ten times the uncertainty in the most precise measurement [2,4]. Adopting this criteria leaves only the half-life from Gr15 to be averaged with the result reported here, yielding $T_{1/2} = 22.448(8)$ s. While this procedure leaves the value for the averaged ^{21}Na half-life unchanged, the uncertainty in the average has increased due to the large discrepancy of nearly 3σ between the ^{21}Na half-lives reported in Gr15 and in this work. The resulting $\chi^2/\nu = 7.4$ for these two measurements carries a p value of only 0.65% and leads to an inflation of the uncertainty in the average by a factor of 2.72 rather than 1.73 if the older and less precise, but more consistent, values are retained.

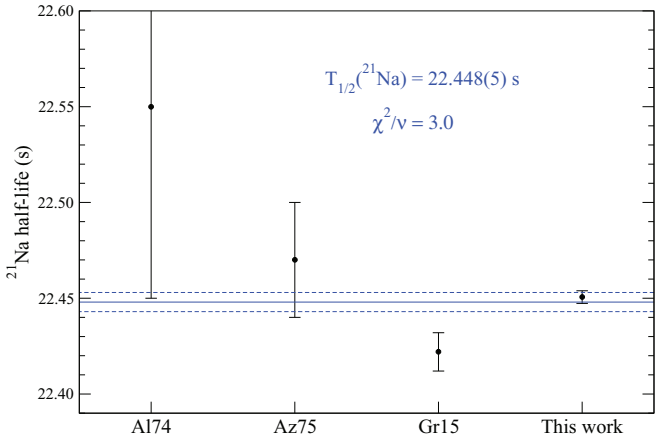

FIG. 9. World-average half-life of ^{21}Na. Shown are measurements from Refs. [7] (Al74), [8] (Az75), [6] (Gr15), and this paper. The result from Ref. [19] has been omitted as it is ∼60 times less precise than this paper, and thus has no impact on either the average half-life or its uncertainty. See text for further discussion.

Combined with world-averaged results for the ^{21}Na Q_{EC} value and branching ratio [20], this world-average ^{21}Na half-life of $T_{1/2} = 22.448(8)$ s yields an $\mathcal{F}t^{\text{mirror}}$ value of:

$$\mathcal{F}t^{\text{mirror}} = 4073.6(40) \text{ s}. \quad (4)$$

The contributions to the ^{21}Na $\mathcal{F}t^{\text{mirror}}$-value error budget are illustrated in Fig. 10. The uncertainty contribution due to the half-life is reduced to the level of the nuclear-structure-dependent theoretical corrections if the world-average evaluation standard is adopted. If the older, less precise half-life measurements are retained in the average, however, the uncertainty contribution due to the half-life surpasses the nuclear-structure-dependent corrections, while it surpasses all other sources of uncertainty if only the result from this paper is retained. In any case the branching ratio is now the only experimental input whose uncertainty has not yet reached the level of the theoretical corrections.

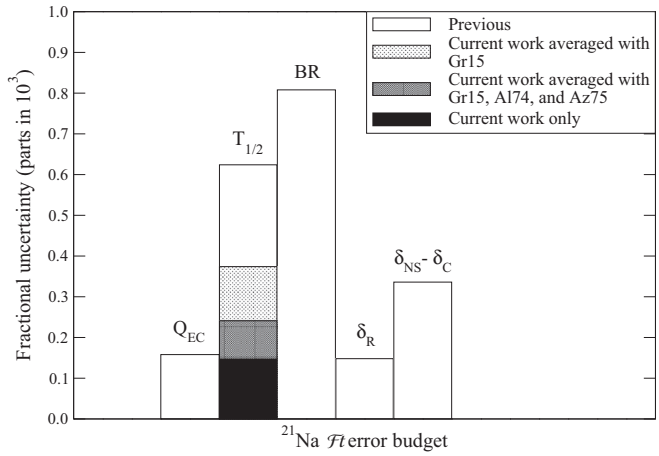

FIG. 10. Fractional uncertainties in the $\mathcal{F}t^{\text{mirror}}$ value for ^{21}Na based on the Q_{EC} value, branching ratio (BR), and half-life from Refs. [20] and [6], the theoretical corrections from Ref. [4], and the half-life value reported here. The different half-life contributions represent the averaging scenarios described in the text. The contribution from the half-life to the $\mathcal{F}t^{\text{mirror}}$ error budget is now comparable to that from the nuclear-structure-dependent corrections if the new (inflated) world average is adopted, and insignificant if the high-precision $T_{1/2}$ result from the present paper is adopted.

Despite the precision achieved in the present paper, the χ^2/ν of 7.4 for the new world-average ^{21}Na half-life is problematic, and with the ultimate goal of producing a robust set of mirror $f_V t$ values further high-precision half-life measurements for ^{21}Na are clearly warranted.

ACKNOWLEDGMENTS

The authors would like to thank the GPS Collaboration and the TRIUMF-ISAC operators and target group. This work was supported by FWO-Vlaanderen (Belgium) and the Natural Sciences and Engineering Research Council of Canada (NSERC). C.E.S. acknowledges support from the Canada Research Chairs program. TRIUMF receives federal funding via a contribution agreement through the National Research Council of Canada (NRC).

[1] M.R. Dunlop *et al.*, Phys. Rev. Lett. **116**, 172501 (2016).
[2] J. C. Hardy and I. S. Towner, Phys. Rev. C **91**, 025501 (2015).
[3] O. Naviliat-Cuncic and N. Severijns, Phys. Rev. Lett. **102**, 142302 (2009).
[4] N. Severijns, M. Tandecki, T. Phalet, and I. S. Towner, Phys. Rev. C **78**, 055501 (2008).
[5] C. Patrignani *et al.* (Particle Data Group), Chin. Phys. C **40**, 100001 (2016).
[6] J. Grinyer *et al.*, Phys. Rev. C **91**, 032501(R) (2015).
[7] D. E. Alburger, Phys. Rev. C **9**, 991 (1974).
[8] G. Azuelos and J. E. Kitching, Phys. Rev. C **12**, 563 (1975).
[9] J. Dilling, R. Krücken, and G. Ball, Hyperfine Interact. **225**, 1 (2014).
[10] A. T. Laffoley *et al.*, Phys. Rev. C **92**, 025502 (2015).
[11] A. P. Baerg, Metrologia **1**, 131 (1965).
[12] E. Browne and J. K. Tuli, Nucl. Data Sheets **111**, 1093 (2010).
[13] M. Wang *et al.*, Chin. Phys. C **36**, 1603 (2012).
[14] V. T. Koslowsky, E. Hagberg, J. C. Hardy, G. Savard, H. Schmeing, K. S. Sharma, and X. J. Sun, Nucl. Instrum. Methods Phys. Res. Sect. A **401**, 289 (1997).
[15] G. F. Grinyer *et al.*, Phys. Rev. C **71**, 044309 (2005).
[16] P. Finlay *et al.*, Phys. Rev. Lett. **106**, 032501 (2011).
[17] V. T. Koslowsky, E. Hagberg, J. C. Hardy, R. E. Azuma, E. T. H. Clifford, H. C. Evans, H. Schmeing, U. J. Schrewe, and K. S. Sharma, Nucl. Phys. A **405**, 29 (1983).
[18] J. M. Chambers, W. S. Cleveland, B. Kleiner, and P. A. Tukey, in *Graphical Methods for Data Analysis* (Wadsworth International Group, Belmont, 1983), p. 62.
[19] S. E. Arnell, J. Dubois, and O. Almén, Nucl. Phys. **6**, 196 (1958).
[20] M. Eibach *et al.*, Phys. Rev. C **92**, 045502 (2015).